



Improvement of the Lateral Distribution Method based on the mixing layer theory



J.N. Fernandes^{a,*}, J.B. Leal^b, A.H. Cardoso^c

^a *Hydraulics and Environment Department, National Laboratory of Civil Engineering, Portugal*

^b *Faculty of Engineering and Science, Universitetet i Agder, Norway and UNIDEMI and Department of Civil Engineering, FCT, Universidade Nova de Lisboa, Portugal*

^c *CEHIDRO and DECivil, Instituto Superior Técnico, Universidade Técnica de Lisboa, Portugal*

ARTICLE INFO

Article history:

Received 17 August 2013

Received in revised form 11 January 2014

Accepted 1 April 2014

Available online 12 April 2014

Keywords:

Compound channels

Floodplain

Main channel

Momentum transfer

Secondary currents

Eddy viscosity

ABSTRACT

The accurate prediction of depth-averaged streamwise velocity, boundary shear stress and lateral shear stress are important requisites for the estimation of the flow depth associated with flood events in compound river channels composed of main channel and floodplain. This engineering problem may be tackled through the analytical solution of the depth-averaged momentum equation. Under uniform flow, this solution relies on the calibration of three descriptors of the bottom friction, secondary currents and lateral shear stress. In this paper, the analytical solution materialized in the Lateral Distribution Method is revisited through the consideration of a new panel division. Accurate measurements of streamwise and spanwise velocities as well as of boundary shear stress are used to obtain new predictors of the coefficients describing the effects of bottom friction, secondary currents and lateral shear.

The new lateral division of the compound channel into four panels is physically based on the mixing layer width, which is computed by an iterative procedure easily implemented in practical applications.

© 2014 Elsevier Ltd. All rights reserved.

1. Introduction and framework of analysis

During floods, rivers frequently acquire a compound channel configuration, which induces important flow interactions between the main channel and the floodplain. The velocity gradient between these flows generates large-scale vortices of quasi-vertical axes (cf. [1]). Depending on the flow depth, one or two longitudinal vortices may also develop near the interface between the main channel and the floodplain due to turbulence anisotropy originated at the fixed boundaries and the interface [2]. The two vortical structures constitute a complex 3D flow structure where momentum transfer between the main channel and the floodplains can easily be identified [3].

In compound channels, the accurate prediction of the lateral distributions of the streamwise velocity and boundary shear stress is rather important. For this reason, several contributions can be found in the literature on the modeling of the compound channel flows. Shiono and Knight [4] derived one analytical solution of the depth-averaged momentum equation for steady uniform flow in the streamwise direction. They have assumed that viscous shear stresses are negligible in comparison with the turbulent shear

stresses and that the time averaged vertical velocity is null. Their solution reads:

$$\rho g h s_0 - \tau_0 \sqrt{1 + 1/s_y^2} = \frac{\partial}{\partial y} [h(\rho UV - \tau_{xy})] \quad (1)$$

where ρ = water density, g = gravity acceleration, h = flow depth, s_0 = longitudinal bottom slope, τ_0 = boundary shear stress, s_y = slope of the main channel lateral-bank (1: s_y = vertical:horizontal), y = lateral position, UV = depth-averaged product of the streamwise and spanwise velocities, respectively, and τ_{xy} = depth-averaged lateral shear stress.

Shiono and Knight [5] added closure models for the boundary shear stress and for the transverse derivative term of the shear stress due to the secondary currents (ρUV) and of the depth-averaged lateral shear stress (τ_{xy}); they also assumed the eddy viscosity approach, according to which:

$$\tau_{xy} = \rho \lambda u_* h \frac{\partial U}{\partial y} \quad (2)$$

where λ = dimensionless eddy viscosity coefficient and $u_* = (\tau_0/\rho)^{1/2}$. Assuming $u_* = (f/8)^{1/2}U$, where f = Darcy–Weisbach friction coefficient, they reduced Eq. (1) into the following ordinary differential equation:

* Corresponding author. Tel.: +351 962422855.

E-mail address: jnfernandes@lnec.pt (J.N. Fernandes).

$$\rho g h s_0 - \frac{1}{8} \rho f U^2 \sqrt{1 + \frac{1}{s_y^2}} + \frac{\partial}{\partial y} \left(\rho \lambda h^2 (f/8)^{1/2} U \frac{\partial U}{\partial y} \right) = \Gamma \quad (3)$$

Here $\Gamma = \rho \frac{\partial}{\partial y} (hUV) =$ secondary current coefficient.

The analytical solution of the momentum equation proposed by Shiono and Knight [5] has been analyzed by several researchers while other analytical solutions have been suggested (e.g. Lambert and Sellin [6] and van Prooijen et al. [7] for uniform flows; Ervine et al. [8] for straight, skewed and meandering overbank flows). In the sequence of the work by Shiono and Knight [5], Abril and Knight [9] have shown that the analytical solution of Eq. (3) is more sensitive to changes of the friction coefficient, f , and of the secondary currents coefficient, Γ , than to those of the dimensionless eddy viscosity coefficient, λ . Omran et al. [10] highlighted the meaning of the secondary flow term in rectangular prismatic channels. These authors revealed that the secondary cells are dependent on the aspect ratio pointed out the difficulty in determining these features.

The analytical solution suggested by Shiono and Knight [5] can be implemented if the channel is adequately divided into panels where the coefficients may be described adequately and appropriate boundary conditions at the limits between panels are correctly specified. These conditions depend on the type and number of panels used in the division. Shiono and Knight [5] proposed the division of the compound channel into three panels: the main channel, the transition region (above the side slope of the main channel) and the floodplain.

For adjacent panels i and $i + 1$, the boundary conditions must guarantee continuous depth-averaged velocity distribution in the spanwise direction, which implies $U_i = U_{i+1}$, $\partial U_i / \partial y = \partial U_{i+1} / \partial y$ and $(h\tau_{xy})_i = (h\tau_{xy})_{i+1}$. The no-slip condition holds for the lateral position at a solid lateral wall, $U_i = 0$. If the channel is symmetric, the lateral gradient of the depth-averaged velocity, $\partial U_i / \partial y$, is zero, in the symmetry axis.

The division of the compound channel must account for the turbulent structure of the flow and the influence of the mixing layer in the region near the interface, where vortices of quasi-vertical axis develop. Defining U_h and U_l as the depth-averaged streamwise velocities out of the mixing layer (corresponding to the higher and lower velocity plateaus, respectively) that develops near the interface between the main channel and the floodplain (cf. Fig. 1), one can also define the lateral position, y_α , where the local depth-averaged streamwise velocity, U_α , reads:

$$U_\alpha = U_l + \alpha(U_h - U_l) \quad (4)$$

for $0 < \alpha < 1$. The mixing layer width, δ , is defined herein according to Pope [11] for plane unbounded mixing layers:

$$\delta = |y_{0.9} - y_{0.1}| \quad (5)$$

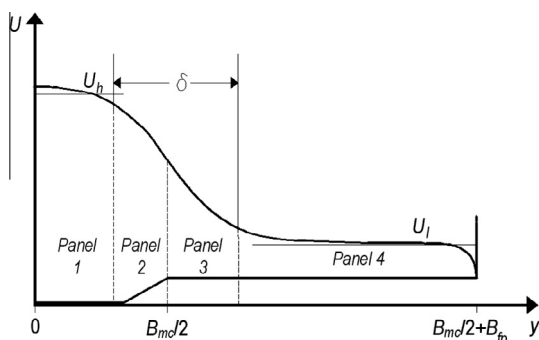


Fig. 1. Definition of plane unbounded mixing layer width, δ . (B_{fp} = floodplain width, B_{mc} = main channel width, U_l and U_h = average streamwise velocities outside the mixing layer in the lower and higher velocity regions).

Preliminary tests carried out in this study have shown that the mixing layer does not extend into the deepest region of the main channel, but it normally extends into the floodplain as schematically shown in Fig. 1, where a new panel division is conceptually presented. The main difference of the new division arises in the floodplain, where, instead of a single panel, a division in two panels, one where the mixing layer influence is felt (Panel 3) and another one where that influence is negligible (Panel 4), is proposed.

In the present paper, the analytical solution of the depth-averaged streamwise momentum equation proposed by Shiono and Knight [5], herein called Lateral Distribution Method (LDM), is analyzed in the framework of the new panel division. An iterative procedure derived from the plane unbounded mixing layer theory (cf. Pope [11]) is adopted to fix the limits of the panels. Measurements of streamwise and spanwise velocities and longitudinal boundary shear stresses taken for nine uniform flows in a straight compound channel with two floodplains roughnesses are used to derive new predictors of the Darcy–Weisbach friction coefficient, f , the dimensionless eddy viscosity coefficient, λ , and the secondary current coefficient, Γ . The new division and the new coefficients are validated through independent experimental data of Zeng et al. [12].

2. Experimental study

2.1. Experimental setup and measuring equipment

The experiments were carried out in a 10 m long and 2 m wide symmetrical compound channel located at the National Laboratory for Civil Engineering in Lisbon, Portugal. According to Fig. 2, its cross section consists of two equal rectangular floodplains (floodplain width $B_{fp} = 0.7$ m) and one trapezoidal main channel (bank full height, $h_b = 0.1$ m, main channel width, $B_{mc} = 0.6$ m, and 45° lateral bank slope, $s_y = 1$). In Fig. 1, h_{fp} and h_{mc} are the floodplain and the main channel flow depths, respectively.

The channel bed is made of polished concrete and its longitudinal slope is $s_0 = 0.0011$ m/m. Six experiments were performed for the original polished concrete bottom (smooth boundary), while another three were run with synthetic grass on the floodplains (rough boundary). Preliminary tests for the characterization of the bed roughness indicated that Manning’s coefficient is $n = 0.0092 \text{ m}^{-1/3} \text{ s}$ for the polished concrete and $n = 0.0172 \text{ m}^{-1/3} \text{ s}$ for the synthetic grass.

Separated inlets for the main channel and for the floodplains were installed by adopting the suggestion of Bousmar et al. [13]. For each inlet, the flow discharge was controlled with a valve and monitored through an electromagnetic flow meter to the accuracy of ± 0.3 l/s. At the downstream end of the flume, independent tailgates for each sub-channel were used to adjust the water levels in the flume.

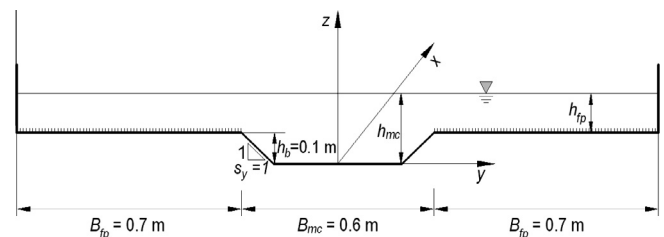


Fig. 2. Schematic representation of the compound channel. (B_{fp} = floodplain width, B_{mc} = main channel width, h_{fp} and h_{mc} = water depth in the floodplain and in the main channel, h_b = bankfull depth and, s_y = slope of the main channel lateral-bank).

Water surface levels were surveyed with a point gauge (accuracy of ± 0.3 mm) in 9 cross sections at 12 lateral positions per cross section.

Velocity measurements were made with a 2D side looking Acoustic Doppler Velocimeter (ADV-vectrino). The acquisition time was fixed in 3 min at each measuring position, at a sampling frequency of 100 Hz. The velocity data were despiked with the filter of Goring and Nikora [14]. Only correlations and signal-to-noise ratio higher than 70% and 15 dB, respectively, were considered. To align the ADV probe with the longitudinal direction, the pitch angle was slightly modified to get $V = 0$ near the floodplain sidewall. This correction was taken into account in the computation of the local mean velocity and the velocity fluctuations (cf. Goring and Nikora [14]). After verifying the symmetry of the flow conditions, only half of the cross section was investigated. In the half cross section, the measuring mesh comprised 22 measuring verticals, 3 measuring points per vertical in the floodplain (between $0.4h_{fp}$ and $0.8h_{fp}$) and 7 in the main channel (between $0.10h_{mc}$ and $h_b + 0.8h_{fp}$). The velocity measurements were taken in a cross section located at $x = 7.5$ m, where the bottom boundary layer and the mixing layer were confirmed to be fully developed.

The boundary shear stress was measured with a Preston tube (external diameter equal to 3.2 mm) connected to a differential pressure transducer in the same cross section ($x = 7.5$ m) and the same lateral positions, y , as the velocity measurements. Patel's calibration curve [16] was used for the smooth boundary cases and the calibration suggested by Hollingshead and Rajaratnam [17] was used for the floodplains covered with synthetic grass. The boundary shear stress records were integrated over the wetted perimeter and the output compared to $\rho g A s_0$, where A stands for the flow cross-section area. The overall absolute deviation was below 6%.

2.2. Control variables and parameters

For a given flow depth, the subsection discharge distribution corresponding to uniform flow is not known *a priori*. An iterative procedure was followed to impose it at $x = 0$ m (cf. [18]). The experimental conditions are listed in Table 1, where apart from the variables previously defined, Q_{mc} and Q_{fp} are the main channel and the floodplain discharges, respectively, and $h_r = h_{fp}/h_{mc}$ stands for the relative floodplain flow depth. The reference of each experiment, included in the first column of Table 1, is to be read as: "hr" followed by "percent relative depth" and by "s" or "r" (for smooth and rough floodplains, respectively). Froude numbers are presented per subsection, $Fr_i = U_i/(gR_i)^{1/2}$, where R is the hydraulic radius and subscript i stands for either main channel, mc , or floodplain, fp . The flow is subcritical for all tests, which is consistent with the use of three independent downstream gates to control the flow depth in each subsection. The Reynolds numbers, $Re_i = 4U_iR_i/\nu$ (ν being the kinematic viscosity) and the floodplain relative roughness, $k/(4R)$ (k being the absolute roughness), are also included in Table 1.

In view of the Reynolds number and the relative roughness of each subsection, it can be concluded that the flow is transition tur-

bulent in the main channel and on the original polished concrete floodplains; it is rough turbulent for the floodplain with synthetic grass.

3. The LDM revisited

3.1. Assessment of the new panel division

The lateral distribution of the depth-averaged streamwise velocities of the uniform flows characterized in Table 1 were used to evaluate the positions $y_{0,1}$ and $y_{0,9}$ as well as the mixing layer width, δ . The values of U_h and U_l are not known *a priori* and the higher and lower plateaus of the velocity were taken as reference. The results are plotted against the relative depth, h_r , in Fig. 3.

The limit of the mixing layer in the region of higher velocity, $y_{0,9}$, is located practically on top of the toe of the main channel bank ($y_{0,9} \approx 0.2$ m, see Fig. 1). Neither the relative depth nor the floodplain roughness seems to interfere with the position $y_{0,9}$. The limit of the mixing layer in the region of lowest velocity, $y_{0,1}$, indicates a slight increase with the relative depth for the smoother floodplains. For the rougher floodplains, $y_{0,1}$ is closer to the upper main channel edge than for smoother floodplains and no clear influence of the relative depth is observed. Due to the increase of the bottom friction and a more efficient energy extraction, when the floodplains are covered with synthetic grass, the mixing layer for floodplains covered with synthetic grass is narrower than it is for smooth floodplains. This difference seems to attenuate with the relative depth, which is ascribable to the decrease of the relative roughness.

In view of the results presented on the mixing layer width, the new division of the compound channel into four panels seems justified (see Fig. 1). The definition of the panels 1 and 2 is the same as in the traditional division. This option is based on the fact the mixing layer edge in the main channel practically coincides with the toe of the bank ($y = 0.2$ m in Fig. 3(a)).

It is clear that mixing spans into a considerable portion of the floodplain width. So, the division between panels 3 and 4 is conceptually placed at the mixing layer border, i.e., at $y = y_{0,1}$. It is postulated here that, in the floodplain, the values of coefficients f , λ and Γ are different inside and outside the mixing layer. As the position $y_{0,1}$ is unknown *a priori*, the hypothesis that the mixing layer spreads into the floodplain to a spanwise position equal to the bank full depth (i.e. $y_{0,1} = B_{mc}/2 + h_{mc}$) is initially assumed. This division is used to divide the compound channel and the analytical results are obtained through Eqs. (4) and (5). Then, a new position for $y_{0,1}$ is calculated based on the predicted lateral distribution of the depth-averaged velocity. The analytical solution is used iteratively until an approximately constant value of $y_{0,1}$ is attained.

3.2. Calibration of f , λ and Γ

Fig. 4 shows the lateral distribution of depth-averaged lateral shear stress:

Table 1
Experimental flow conditions.

Flow reference	Floodplain flow	h_{mc} (m)	h_r (-)	Q_{mc} (L.s ⁻¹)	Q_{fp} (L.s ⁻¹)	Fr_{mc}	Fr_{fp}	$Re_{mc} (\times 10^5)$	$Re_{fp} (\times 10^5)$	Floodplain relative roughness, $k/(4R)$
hr10s	Transition turbulent	0.1119	0.11	34.9	3.3	0.67	0.58	2.02	0.09	0.0032
hr15s	Transition turbulent	0.1172	0.15	38.8	6	0.69	0.61	2.25	0.17	0.0022
hr20s	Transition turbulent	0.1220	0.19	42.2	11.2	0.70	0.78	2.45	0.31	0.0017
hr25s	Transition turbulent	0.1309	0.24	46.7	18.6	0.69	0.80	2.71	0.50	0.0012
hr30s	Transition turbulent	0.1402	0.30	54.2	26.4	0.70	0.76	3.17	0.66	0.0009
hr38s	Transition turbulent	0.1600	0.38	67.8	50.5	0.71	0.82	3.93	1.32	0.0006
hr15r	Rough turbulent	0.1192	0.15	35.1	3.7	0.61	0.32	2.04	0.10	0.0885
hr20r	Rough turbulent	0.1244	0.21	39.3	7.3	0.63	0.44	2.28	0.20	0.0697
hr30r	Rough turbulent	0.1450	0.31	42.3	16.6	0.52	0.41	2.45	0.44	0.0378

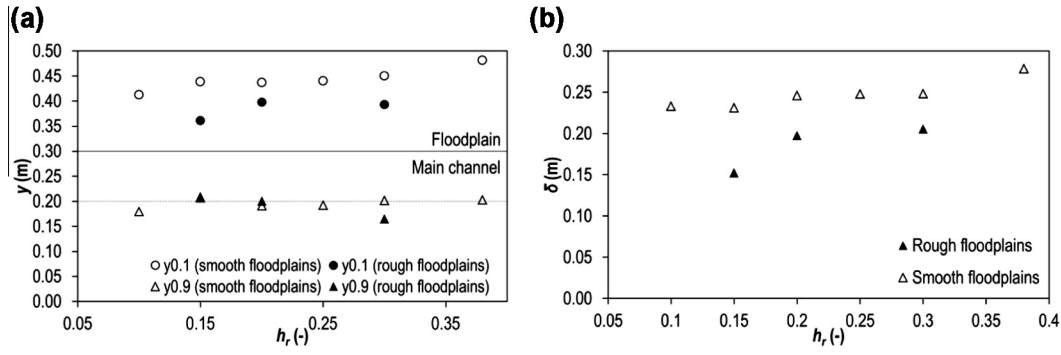


Fig. 3. (a) Positions $y_{0,1}$, and $y_{0,9}$ and (b) mixing layer width, δ .

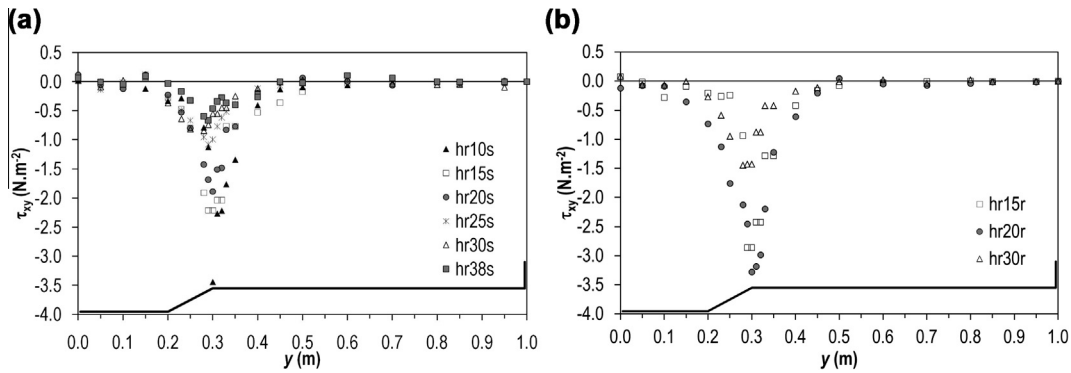


Fig. 4. Lateral distribution of the depth-averaged lateral shear stresses, τ_{xy} , for experiments with (a) floodplains made of polished concrete and (b) floodplains covered by synthetic grass.

$$\tau_{xy} = 1/h \int_0^h (-\rho \overline{u'v'}) dz \quad (6)$$

for both floodplain roughnesses.

For all flow cases, the distribution displays a peak at the main channel edge. For a given relative depth, the depth-averaged lateral shear stresses seem stronger over the rough bed. Sufficiently far from the interface, the depth-averaged lateral shear stresses are close to zero. As the relative depth increases, the velocity gradient between the main channel and the floodplain decreases, inducing the reduction of the magnitude of the lateral shear stress peaks.

Eq. (2) was used to obtain the experimental dimensionless eddy viscosity coefficient, λ . As $\partial U/\partial y$ is very sensitive to experimental inaccuracies on the streamwise velocity distribution, the derivative was estimated by applying a second order polynomial to every five consecutive points. The results of the dimensionless eddy viscosity are shown in Fig. 5 for both floodplain roughnesses.

In the figure, the horizontal lines represent the averaged values of λ per panel, for flow cases hr10s and hr15r (dashed lines), hr38s and hr30r (solid lines). In spite of the scatter, it may be concluded that: (i) the values of λ are higher in the floodplain than in the main channel; (ii) approximately constant values are observed in the main channel irrespective of the relative depth, whereas higher values are observed in the floodplain for smaller relative depths; (iii) no clear dependence on the roughness of the floodplain is observed.

Fig. 6 presents the values of the Darcy–Weisbach friction coefficient, f , obtained from the boundary shear stress measurements as $f = 8\tau_0/(\rho U^2)$.

Fig. 6 also presents horizontal lines corresponding to the values of f per subsection, for flow cases hr10s and hr15r (solid lines), hr38s and hr30r (dashed lines). These values of $f = 8gn^2/R^{1/3}$ were

obtained by imposing the n values issued from single channel experiments. It seems reasonable to conclude that this approach can satisfactorily describe the average value of f in a given subsection (main channel or floodplain). Higher discrepancies are found within the mixing layer, especially for small relative depths. Although the bottom turbulence and, consequently, f is affected by secondary currents and by the mixing layer turbulence (cf. [3,7]), the lateral variation of f in each subsection is not considered here and the boundary shear stress is simply described through the Manning coefficient, n .

In the present work, the accuracy of the ADV vectrino was not sufficient to measure the oscillations of the very small spanwise velocity components. Due to the small magnitude of this velocity, a very small misalignment invalidates accurate measurements [15]. Consequently, the derivative of the depth-averaged spanwise velocity, V , could not be evaluated. Instead of calculating Γ as $\rho \partial(HUV)/\partial y$, the secondary currents coefficient was obtained, for each uniform flow, through the balance given by Eq. (1), where both the lateral shear stress (Fig. 4) and the boundary shear stress (measured with Preston tube) are known.

The issuing apparent shear stresses due to the secondary flow, $-\rho UV$, are shown in Fig. 7 for both floodplains roughnesses.

In the main channel, the apparent shear stress decreases with y in a similar way for all depths with the same floodplain roughness. It reaches a negative peak at the edge of the main channel. A quasi-linear increase of $-\rho UV$ is observed in the floodplain for all flow cases; as compared with the main channel, a bigger scatter prevails and no systematic influence of h_r is identified.

Fig. 8 shows the lateral distribution of the secondary currents coefficient, Γ , scaled by $\rho g h s_0$, for both floodplain roughnesses. Horizontal dashed lines represent the averaged values of $\Gamma/(\rho g H s_0)$ in the four panels division proposed above. It is clear

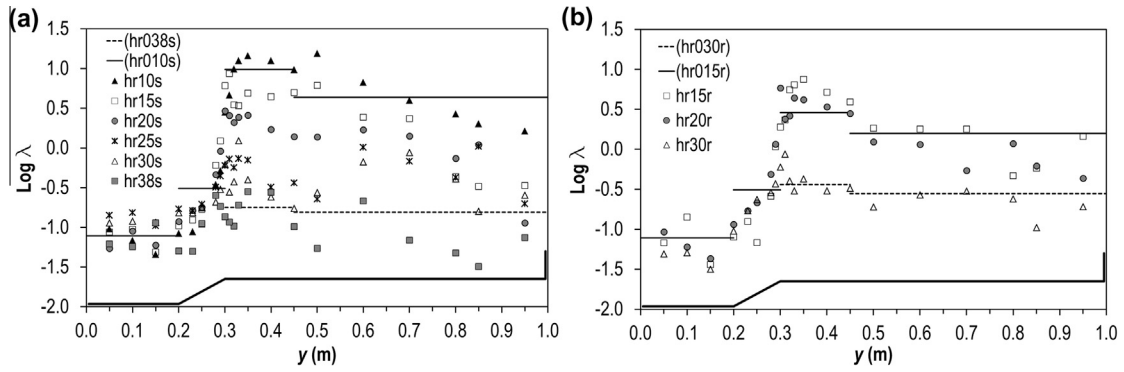


Fig. 5. Dimensionless eddy viscosity, λ , coefficient for experiments with (a) floodplains made of polished concrete and (b) floodplains covered by synthetic grass.

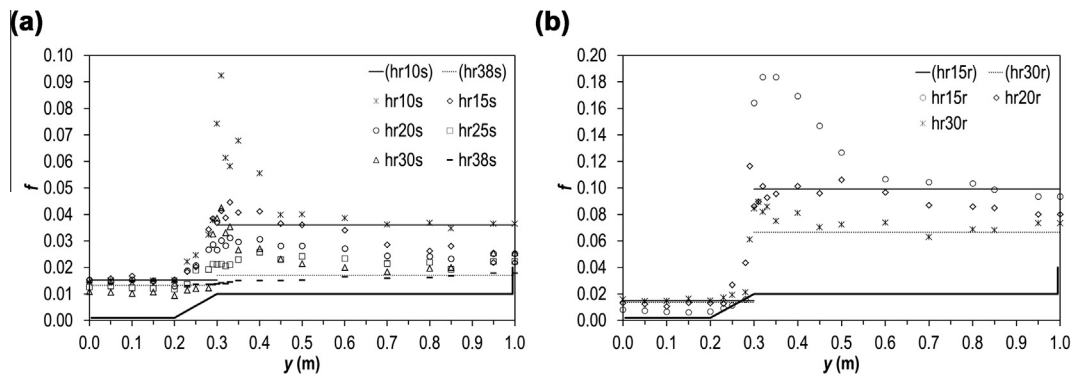


Fig. 6. Darcy–Weisbach coefficient, f , for experiments with (a) floodplains made of polished concrete and (b) floodplains covered by synthetic grass.

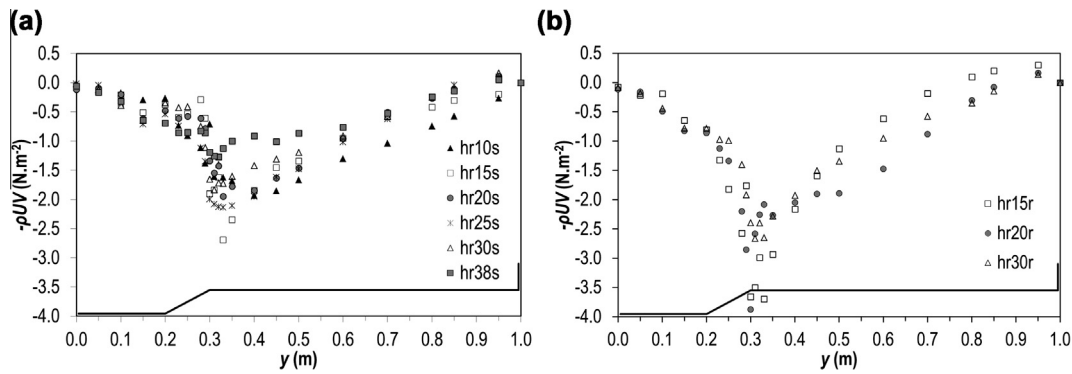


Fig. 7. Lateral distribution of the apparent shear stress, due to the secondary flow for the experiments with (a) floodplains made of polished concrete and (b) floodplains covered by synthetic grass. (U and V = average streamwise and spanwise velocities).

that approximately constant values of $\Gamma/(\rho g H s_0)$ are observed far from the main channel bank.

From the previous discussion, the following conclusions can be drawn:

1. The dimensionless eddy viscosity coefficient, λ , is the same for both bottom roughnesses. It does not depend on the relative depth in the main channel (Panels 1 and 2) while it does in the floodplain (Panels 3 and 4), according to Table 2.
2. The Darcy–Weisbach friction factor can be obtained by $f = 8gn^2/R^{1/3}$. It renders a single value for the main channel (Panels 1 and 2) and a different value for the floodplain (Panels 3 and 4) per relative depth and type of bottom roughness (cf. Fig. 6).

3. Non-dimensional values of the secondary currents coefficient, Γ , vary from panel to panel and depend on the bottom roughness (cf. Table 2).

4. Validation of the improved LDM

The LDM results of the depth-averaged streamwise velocity for both the traditional division (three panels) and the new division (four panels) are compared with the experimental data in Fig. 9. For the floodplain, the calibrated values of Γ and λ used with the traditional division were -0.35 and $0.078(2h_r)^{-2.9}$, respectively (for both parameters, the effect of the floodplain roughness was not distinguished). The results of the boundary shear stress and

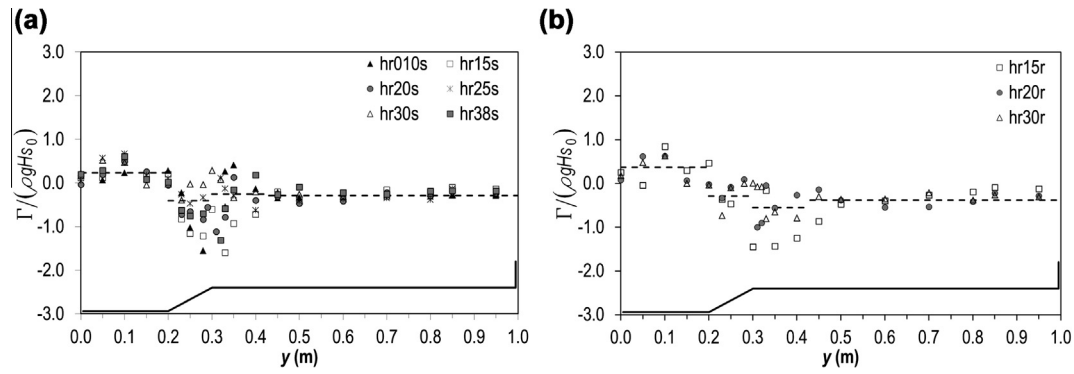


Fig. 8. Lateral distribution of the secondary currents coefficient, Γ , with (a) floodplains made of polished concrete and (b) floodplains covered by synthetic grass. (H = water depth and s_0 = longitudinal slope).

Table 2
Secondary currents and dimensionless eddy viscosity coefficients for each panel.

Floodplain	$\Gamma/(\rho g H s_0)$				λ			
	Panel 1	Panel 2	Panel 3	Panel 4	Panel 1	Panel 2	Panel 3	Panel 4
Polished concrete	0.23	-0.41	-0.26	-0.29	0.078	0.31	$0.078(2h_r)^{-3}$	$0.078(2h_r)^{-2.5}$
Synthetic grass	0.37	-0.29	-0.55	-0.38				

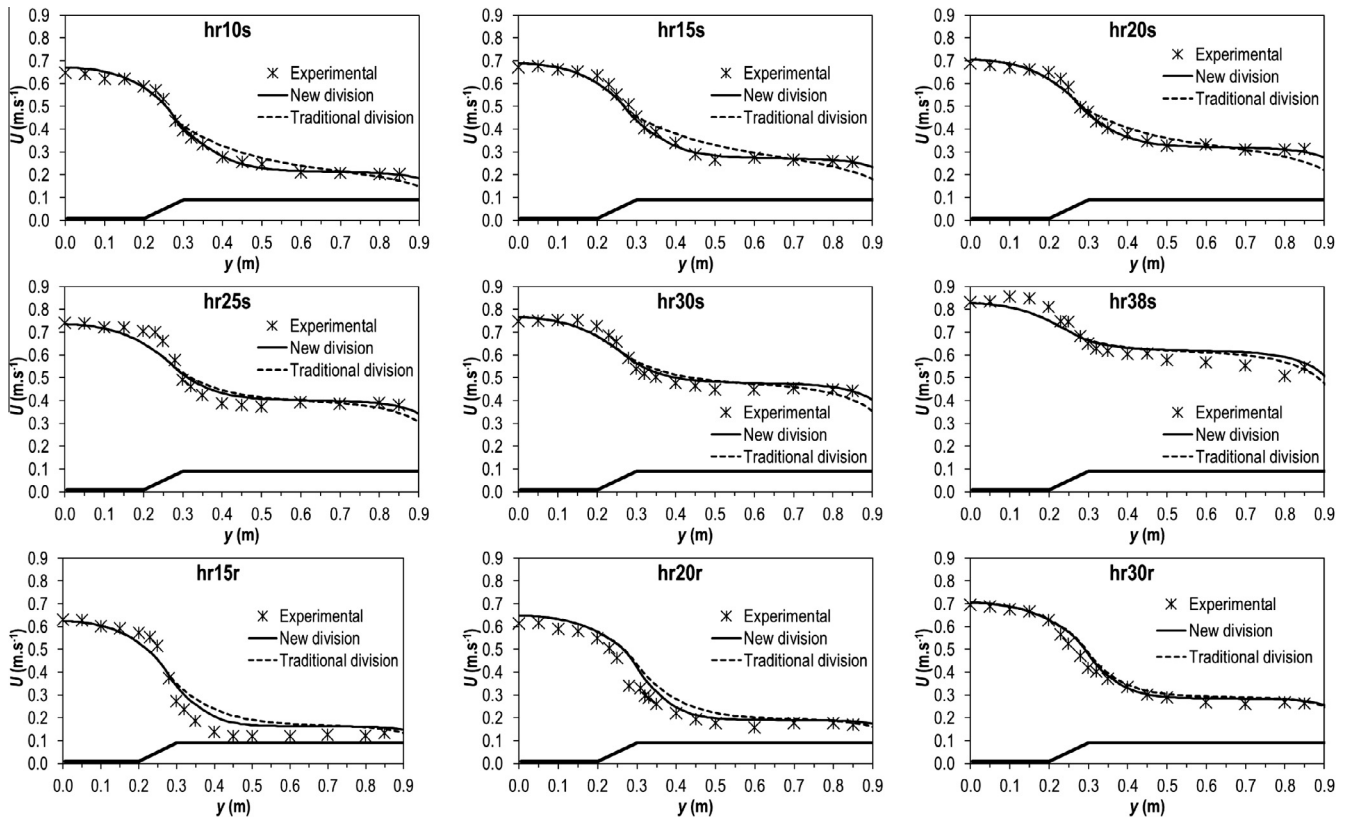


Fig. 9. Lateral distribution of the depth-averaged velocity, U .

of the depth-averaged lateral shear stress are presented in Figs. 10 and 11, respectively.

The averaged deviation, $\Delta\psi$, of each predicted variable (depth-averaged streamwise velocity, boundary shear stress and depth-averaged lateral shear stress) was calculated as:

$$\Delta\psi = \frac{\sqrt{\sum_i^N (\psi_i^m - \psi_i^p)^2}}{N} \quad (7)$$

where ψ_i^m and ψ_i^p are, respectively, the measured and predicted value of each variable at a given lateral position and N is the number of positions. The results on U , τ_0 and τ_{xy} for the traditional and the new divisions are presented in Table 3.

The experimental data and the predicted depth-averaged streamwise velocities show a good agreement for almost all flow cases. Overall, the averaged deviation in the prediction of the depth-averaged streamwise velocities is reduced when the new

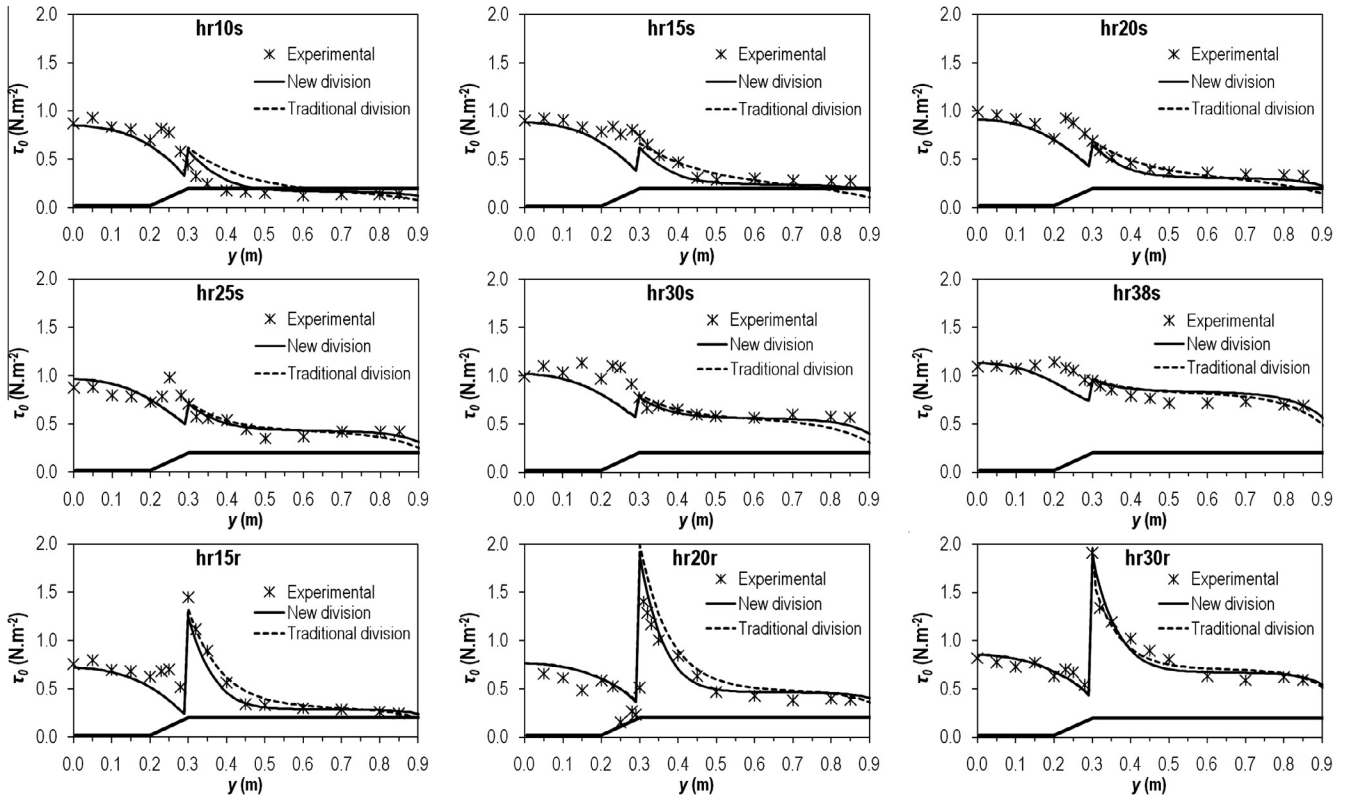


Fig. 10. Lateral distribution of the boundary shear stress, τ_0 .

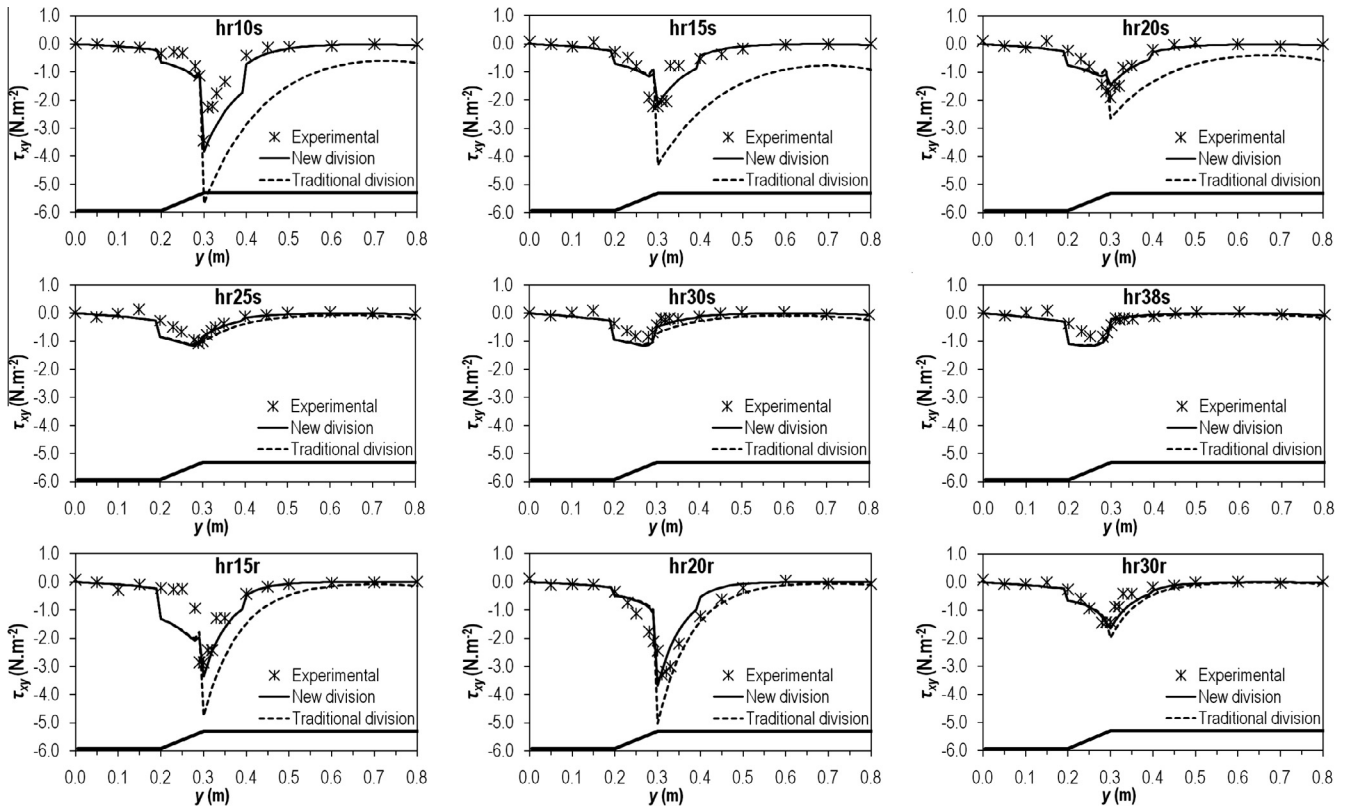
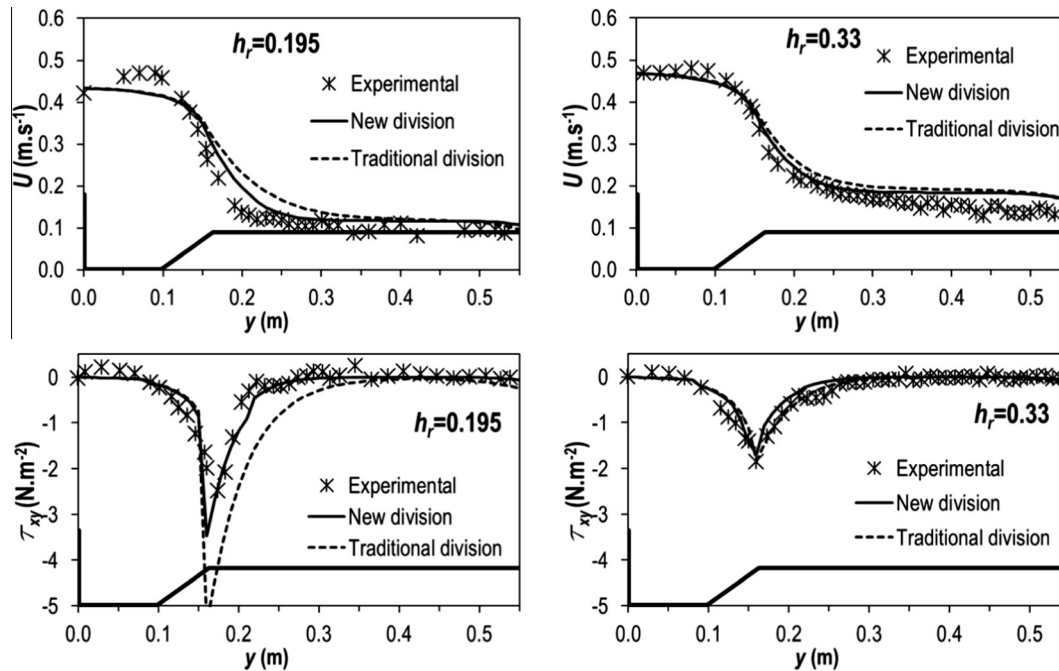


Fig. 11. Lateral distribution of the depth-averaged lateral shear stress, τ_{xy} .

Table 3

Averaged deviation in the prediction of each variable.

Variable	Division	hr10s	hr15s	hr20s	hr25s	hr30s	hr38s	hr15r	hr20r	hr30r
U	New	0.006	0.003	0.005	0.010	0.007	0.012	0.012	0.024	0.020
	Traditional	0.009	0.008	0.009	0.011	0.009	0.013	0.014	0.025	0.021
τ_0	New	0.026	0.028	0.119	0.028	0.032	0.026	0.057	0.087	0.101
	Traditional	0.031	0.028	0.189	0.030	0.034	0.026	0.057	0.091	0.101
τ_{xy}	New	0.172	0.167	0.028	0.076	0.094	0.073	0.176	0.238	0.118
	Traditional	0.349	0.299	0.029	0.087	0.101	0.076	0.237	0.272	0.128

**Fig. 12.** Results of the depth-averaged velocity and of the lateral shear stress, experimental results by Zeng et al. [12].

division is applied. The division into four panels leads to improved results especially for the smaller relative depths (hr10s, hr15s, hr20s), near to the floodplain edge, where the mixing layer influence is important.

In case hr25s, the shape of the lateral distribution of the depth-averaged streamwise velocity in the mixing layer is not well predicted. For flow hr15r the depth-averaged velocity in the floodplain is over-predicted, which may be due to the assumption of constant value of f in all the floodplain width, as discussed in the boundary shear stress section.

In general, the simulated results of the boundary and lateral shear stresses show good agreement with the experimental data. For the lower relative depths, the simulations are particularly accurate. Correct location and magnitude of the peak of the lateral shear stress are obtained in the simulations. The new division of the compound channel into four panels leads to a remarkable improvement in the prediction of the lateral distribution of the lateral shear stress (see Fig. 11), possibly because it incorporates the effects of the mixing layer on the floodplain region. On the contrary, equivalent predictions of the boundary shear stress were obtained with both divisions, which comes to no surprise since the lateral distribution of f is equal in both cases (see Fig. 6).

The applicability of the proposed division as well as of the new proposals regarding the dimensionless eddy viscosity and secondary currents coefficients was assessed by comparing the results of the LDM with the experimental results presented by Zeng et al. [12]. These authors carried out experiments in a 1.218 m wide symmetric and trapezoidal compound channel. Other main charac-

teristics of the channel are $B_{mc} = 0.163$ m, $h_b = 0.065$ m, $s_y = 1$, $B_{fp} = 0.446$ m and $s_0 = 0.00123$. The main channel was made of glass ($n_{mc} = 0.009$ m^{-1/3} s) and the floodplains were covered with pebbles with a median diameter of 5.75 mm ($n_{fp} = 0.02$ m^{-1/3} s). Two experiments under uniform flow were performed with relative depths, h_r , equal to 0.195 and to 0.330. The lateral distributions of depth-averaged streamwise velocity and lateral shear stress were measured.

The experimental and analytical results for the depth-averaged streamwise velocity and for the lateral shear stress are presented in the Fig. 12. The results have been obtained with the coefficients calibrated in the present experimental study; the new and the traditional divisions were applied.

The results show that the coefficients calibrated with the uniform flows presented in Table 1 lead to a rather good prediction of the depth-averaged streamwise velocity as well as of the lateral shear stress. Above all, it is observed that the new division of the compound channel into four panels improves the prediction of the streamwise depth-averaged velocity and lateral shear stress as compared to the traditional division into three panels, especially for small relative depths. These results confirm the robustness of the improved Lateral Distribution Method.

5. Conclusions

In the present paper, the analytical solution of the depth-averaged streamwise momentum equation proposed by Shiono and

Knight [5] is revisited and a new division of the compound channel is proposed, based on the width of the mixing layer. It consists on the division of the floodplain into two panels instead of the traditional use of a single one. The calibration of the friction factor and dimensionless eddy viscosity and secondary currents coefficients in each panel was obtained through measurements of velocities and boundary shear stress for two roughnesses in the floodplain.

Accurate predictions of depth-averaged streamwise velocity and lateral and boundary shear stresses were obtained for all flow cases. An improvement of the results as compared with those obtained through the traditional division is documented for small relative depths, especially regarding the depth-averaged streamwise velocity and the lateral shear stress.

The new coefficients and the proposed division were also tested against the experimental data presented by Zeng et al. [12]. Accurate results of depth-averaged velocity and lateral shear stress were obtained, highlighting the validity of the method for different setups and flow conditions. For different geometries, the proposed panel division can be used as far as the parameters can be calibrated against known distributions of the depth-averaged velocities.

Acknowledgments

The authors wish to acknowledge the financial support of the Portuguese Foundation for Science and Technology through the project PTDC/ECM/70652/2006. The first author acknowledges the support of the Portuguese Foundation for Science and Technology through the Grant No. SFRH/BD/37839/2007.

References

- [1] Sellin RHJ. A laboratory investigation into the interaction between the flow in the channel of a river and that over its floodplain. *La Houille Blanche* 1964;7:793–802. <http://dx.doi.org/10.1051/lhb/1964044>.
- [2] Tominaga A, Nezu I. Turbulent structure in compound open-channel flows. *J Hydraulic Eng* 1991;117(1):21–41. [http://dx.doi.org/10.1061/\(ASCE\)0733-9429\(1991\)117:1\(21\)](http://dx.doi.org/10.1061/(ASCE)0733-9429(1991)117:1(21)).
- [3] Nezu I, Nakayama T. Space-time correlation structures of horizontal coherent vortices in compound channel flows by using particle-tracking velocimetry. *J Hydraulic Res* 1997;35(2):191–208. <http://dx.doi.org/10.1080/00221689709498426>.
- [4] Shiono K, Knight DW. Two-dimensional analytical solution for compound channel. In: *Proceedings of 3rd international symposium on refined flow modelling and turbulence measurements*. Academy Press; 1989. p. 591–9.
- [5] Shiono K, Knight DW. Turbulent open channel flows with variable depth across the channel. *J Fluid Mech* 1991;222:617–46. <http://dx.doi.org/10.1017/S0022112091001246>.
- [6] Lambert MF, Sellin RHJ. Discharge prediction in straight compound channels using the mixing length concept. *J Hydraulic Res* 1996;34(3):381–94. <http://dx.doi.org/10.1080/00221689609498487>.
- [7] van Prooijen B, Battjes J, Uijttewaai W. Momentum exchange in straight uniform compound channel flow. *J Hydraulic Eng* 2005;131(3):75–183. [http://dx.doi.org/10.1061/\(ASCE\)0733-9429\(2005\)131:3\(175\)](http://dx.doi.org/10.1061/(ASCE)0733-9429(2005)131:3(175)).
- [8] Ervine DA, Babaayan-Koopaei K, Sellin RHJ. Two dimensional solution for straight and meandering overbank flows. *J Hydraulic Eng* 2000;126(9):653–69. [http://dx.doi.org/10.1061/\(ASCE\)0733-9429\(2000\)126:9\(653\)](http://dx.doi.org/10.1061/(ASCE)0733-9429(2000)126:9(653)).
- [9] Abril JB, Knight DW. Stage-discharge prediction for rivers in flood applying a depth-averaged model. *J Hydraulic Res* 2004;42(6):616–29. <http://dx.doi.org/10.1080/00221686.2004.9628315>.
- [10] Omran M, Knight DW, Beaman F, Morvan H. Modelling equivalent secondary current cells in rectangular channels. In: Altınakar MS, Kokpinar MA, Aydin I, Okgar SC, Kirkgöz S, editors. *RiverFlow 2008*, vol. 1. Cesme, Turkey; 2008. p. 75–82. ISBN: 978-605-60136-1-4.
- [11] Pope SB. *Turbulent flows*. Cambridge University Press; 2000. pp. 139–144. <http://dx.doi.org/10.1088/1468-5248/1/1/702>.
- [12] Zeng YH, Guymier I, Spence KJ, Huai WX. Application of analytical solutions in trapezoidal compound channel flow. *River Res Appl* 2012;28:53–61. <http://dx.doi.org/10.1002/rra.1433>.
- [13] Bousmar D, Rivière N, Proust S, Paquier A, Morel R, Zech Y. Upstream discharge distribution in compound-channel flumes. *J Hydraulic Eng* 2005;131(5):408–12. [http://dx.doi.org/10.1061/\(ASCE\)0733-9429\(2005\)131:5\(408\)](http://dx.doi.org/10.1061/(ASCE)0733-9429(2005)131:5(408)).
- [14] Goring DG, Nikora VI. Despiking acoustic Doppler velocimeter records. *J Hydraulic Eng* 2002;128(1):117–26. [http://dx.doi.org/10.1061/\(ASCE\)0733-9429\(2002\)128:1\(117\)](http://dx.doi.org/10.1061/(ASCE)0733-9429(2002)128:1(117)).
- [15] Roy AG, Biron P, de Serres B. On the necessity of applying a rotation to instantaneous velocity measurements in river flows. *Earth Surf Proc Land* 1996;21(9):817–27. [http://dx.doi.org/10.1002/\(SICI\)1096-9837\(199609\)21:9](http://dx.doi.org/10.1002/(SICI)1096-9837(199609)21:9).
- [16] Patel VC. Calibration of the Preston tube and limitations on its use in pressure gradients. *J Fluid Mech* 1965;23(1):185–208. <http://dx.doi.org/10.1017/S0022112065001301>.
- [17] Hollingshead AB, Rajaratnam N. A calibration chart for the Preston tube. *J Hydraulic Res* 1980;18(4):313–26. <http://dx.doi.org/10.1080/00221688009499538>.
- [18] Fernandes JN, Leal JB, Cardoso AH. Analysis of flow characteristics in a compound channel: comparison between experimental data and 1D numerical simulations, urban environment series. In: Rauch Sébastien, Morrison Gregory M, editors. *Proceedings of the 10th urban environment symposium*. Elsevier; 2012. <http://dx.doi.org/10.1007/978-94-007-2540-9-23>.